Published in final edited form as:
Electrochim Acta. 2014 December 20; 150: 99–107. doi:10.1016/j.electacta.2014.10.136.

Graphene-based biomimetic materials targeting urine metabolite as potential cancer biomarker: application over different conductive materials for potentiometric transduction

Liliana A.A.N.A. Truta, **Nádia S. Ferreira**, and **M. Goreti F. Sales***
BioMark, Sensor Reasearch/ISEP, School of Engineering, Polytechnic Institute of Porto, Portugal

Abstract

This works presents a novel surface Smart Polymer Antibody Material (SPAM) for Carnitine (CRT, a potential biomarker of ovarian cancer), tested for the first time as ionophore in potentiometric electrodes of unconventional configuration. The SPAM material consisted of a 3D polymeric network created by surface imprinting on graphene layers. The polymer was obtained by radical polymerization of (vinylbenzyl)trimethylammonium chloride and 4-styrenesulfonic acid (signaling the binding sites), and vinyl pivalate and ethylene glycol dimethacrylate (surroundings). Non-imprinted material (NIM) was prepared as control, by excluding the template from the procedure. These materials were then used to produce several plasticized PVC membranes, testing the relevance of including the SPAM as ionophore, and the need for a charged lipophilic additive. The membranes were casted over solid conductive supports of graphite or ITO/FTO. The effect of pH upon the potentiometric response was evaluated for different pHs (2-9) with different buffer compositions.

Overall, the best performance was achieved for membranes with SPAM ionophore, having a cationic lipophilic additive and tested in HEPES (4-(2-hydroxyethyl)-1-piperazineethanesulfonic acid) buffer, pH 5.1. Better slopes were achieved when the membrane was casted on conductive glass (−57.4mV/decade), while the best detection limits were obtained for graphite-based conductive supports (3.6×10^{-5}mol/L). Good selectivity was observed against BSA, ascorbic acid, glucose, creatinine and urea, tested for concentrations up to their normal physiologic levels in urine. The application of the devices to the analysis of spiked samples showed recoveries ranging from 91% (± 6.8%) to 118% (± 11.2%). Overall, the combination of the SPAM sensory material with a suitable selective membrane composition and electrode design has lead to a promising tool for point-of-care applications.

Keywords

Carnitine; Surface Molecular imprint; Charged binding Sites Graphene; Solid conductive supports; Potentiometry; Urine

*Address correspondence to Goreti Sales, BioMark, Sensor Reasearch/ISEP, School of Engineering, Polytechnic Institute of Porto, R. Dr. António Bernardino de Almeida, 431, 4200-072 Porto, Portugal. Tel: +351 228 340 544; Fax: +351 228 321 159. goreti.sales@gmail.com or mgf@isep.ipp.pt.

1. Introduction

Ovarian cancer is also called the “silent killer” because it is hardly detected and the deadliest of all gynecologic cancers. Early detection may be achieved by early screening of specific biomarker compounds bearing a predictive value. Because ovarian tissues can be transformed into several quaternary amines [1], the presence of carnitine (CRT) in urine may be correlated to ovarian cancer [1; 2]. CRT is a quaternary amine, with a fundamental role in the mitochondrial β-oxidation of long-chain fatty acids by enabling their transport into the mitochondrial matrix [3]. Is also acts as an antioxidant, contributing to maintain the normal function of the cells and protect cells from oxidative stress conditions related to cardiovascular diseases, heart and renal failure [4] and diabetes [5]. Furthermore, CRT is an inhibitor of cisplatin-induced injury of the kidney and small intestine and, hence, it may have therapeutic potential in cancer [6].

Numerous analytical methods have been described in the literature to determine CRT in different biological samples such as chromatography [7; 8; 9; 10; 11], radiometry assays [9], electrophoresis [12; 13; 14], fluorimetry and spectrophotometry [15; 16], electrochemical assays with potentiometric [17; 18; 19], and amperometric [20] or Quartz-crystal microbalance transduction [21]. Overall, these methods are effective but unsuitable for point-of-care applications, where response time, portability and cost are critical. In clinical context, immunoassays are today dominant for ensuring highly selective readings of the target biomolecule. This high selectivity accounts the use of antibodies as bioreceptor material, but this is also coupled to slow and expensive procedures [22]. An alternative to conventional immunoassays, such as ELISA, could be the development of a biomimetic material, acting as plastic antibody, and its use in the construction of a biosensor device.

The production of plastic antibodies makes use of molecular imprinting technology, where a biomolecule is imprinted within a polymeric network. In general, the resulting biomimetic nanostructures display good sensitivity/selectivity for the target compound, while ensuring high mechanical strength, robustness, low cost, reusability, and low response time. Surface imprinting is the technique of choice for avoiding hindered diffusion of the imprinted template from the polymeric matrix [23; 24]. The inclusion of charged binding sites to create Smart Polymer Antibody Material (SPAM) surfaces is a recent and successful approach, where the binding positions are complementary to the template both in shape and in charge [25]. Since these sites are designed in a neutral network environment, the affinity/selectivity of the template for its binding/charged site becomes enhanced.

Different nanostructures have been employed to support such biomimetic structures, varying from silica [26; 27] to gold [28; 29]or carbon allotropes [30; 31]; when electrical transduction is intended, the use of highly conductive materials of low cost is preferred, being graphene an emerging material under this context. Graphene is a single-layer sheet of sp^2 hybridized carbon atoms arranged in a two-dimensional nanostructure [32], bearing outstanding electrical properties, as well as thermal stability and mechanical strength [32; 33]. The easy functionalization of graphene is also a key facture for its compatibility in bio/nano interfaces, justifying its intensive and emerging use [33].

Moreover, the association of plastic antibodies to ion-selective electrodes (ISEs) has been proven an advantageous approach in electrical transduction, not only for the detection of small biomolecules [34], but also for high dimension bio-structures such as protein biomarkers [30]. ISEs are portable and low-cost devices for field applications, providing selective, precise, rapid and sensitive responses over a broad range of concentration of ionic analytes [35]. The use of conductive solid support has shown a successful approach for preparing ISE, enabling an easy handling of the electrode by eliminating its conventional internal solution. In this context, it would be interesting to understand the changes arising by replacing the regular graphite-base conductive support by conductive glass/plastic. These are today low cost materials, readily available in the market, and could allow replacing the conventional “pen” configuration of ISEs by flat transparent surfaces were half area is electrically active.

Thus, this work describes for the first time a SPAM nanostructure assembled on graphene for the detection of CRT metabolite in urine. This material was created by growing a neutral reticulated polymer by radical polymerization of vinyl pivalate (VPi) cross-linked with ethylene glycol dimethacrylate (EGDMA). The charged positions were signed with (vinylbenzyl)trimethylammonium (VBTMA) chloride and 4-styrenesulfonic acid (SSA) sodium salt. The obtained materials were included in plasticized PVC selective membranes to act as ionophore in potentiometric transduction, using different conductive solid supports. Several membrane compositions were produced to ensure that the device would display suitable analytical features. The overall analytical performance was evaluated and the membrane composition optimized, leading ultimately to a successful application of the device to the analysis of CRT in biological samples.

2. Experimental

2.1. Equipment and Materials

All electromotive force (emf) measurements were made at room temperature and under constant stirring in a Crison pH-meter, GLP21, decimilivoltammeter (±0.1mV sensitivity) connected to a reference electrode, also from Crison, 5240, or to double-junction combined glass electrode Consort. A Sonorex digitec sonicater from Bandelin, and/or a vortex from Citomed (C 1301B-230V) were used to promote the dissolution of the solids and homogenization of the solutions/suspensions.

Solid materials were characterized by Fourier Transform Infrared Spectrometry (FTIR), using a Nicolet iS10 FTIR spectrometer, from Thermo Scientific, equipped with an Attenuated Total Reflectance (ATR) sampling accessory of diamond contact crystal, also from Nicolet. The same solids were also analyzed by Raman Spectroscopy, using the Confocal Raman Microscope a300M+ from WITec GmbH, equipped with an objective 50× Zeiss NA=0.70 and operating in single spectrum mode, at 532 nm laser.

Indium tin oxide (ITO) coated PET (polyethylene terephthalate), surface resistivity 60 Ω/sq, and Fluorine doped (FTO) tin oxide coated glass slide, surface resistivity ~7 Ω/sq, were purchased from Sigma-Aldrich, cut in pieces (~1×1cm) for electrical wiring and selective membrane deposition.

2.2. Reagents and solutions

All chemicals were of analytical grade and deionised water (conductivity <0.1 μS.cm^{-1}) was employed. CRT hydrochloride, 4-(2-hydroxyethyl)-1-piperazineethanesulfonic acid (HEPES), bovine serum albumin (BSA), Piperazine-*N*,*N*′-bis(2-ethanesulfonic acid) (PIPES) and VPi were obtained from Sigma-Aldrich; Creatinine (Crea), *N*-(3-dimethylaminopropyl)-*N*′-ethylcarbodiimide hydrochloride (EDAC), *N*-Hydroxysuccinimide (NHS), *o*-nitrophenyloctyl ether (*o*NPOE), poly(vinylchloride) (PVC) of high molecular weight and potassium *tetrakis*(4-chlorophenyl)borate (TpClPB) from Fluka; Tetrahydrofuran (THF), ascorbic acid and sodium phosphate dibasic dihydrate ($Na_2HPO_4.2H_2O$) from Riedel-deHäen; Hydrochloric acid and *tris*(hydroxymethyl)aminomethane (TRIS), potassium di-hydrogenphosphaste (KH_2PO_4) and sodium chloride (NaCl) were from Panreac, *p*-tetraoctilammonium bromide (*p*TOAB) and VBTMA chloride 97% to Acrös Organics; 4-Morpholinepropanesulfonic acid, sodium salt (MOPS) to AppliChem; Ammonium persulfate (APS) was obtained from JVP; SSA sodium salt and 2-(N-morpholino)ethanesulfonic acid (MES) from Alfa Aesar; glacial Acetic acid from Carlo Erba; Dextrose anhidrous (Glucose) from Fisher BioReagents; EGDMA and sodium dodecyl sulfate (electrophoresis) (SDS) from TCI; Potassium nitrate from Pronalab; Hydrogen peroxide and potassium chloride (KCl) from Merck; Sulphuric acid from Scharlau; Potassium permanganate from BDH; and Urea was produced from Fagron.

The Phosphate buffered saline (PBS) solution, with pH adjusted to 7.4, was prepared by the dissolution of 6.8×10^{-2} mol/L NaCl, 1.4×10^{-3} mol/L KCl, 3.3×10^{-3} mol/L $Na_2HPO_4.2H_2O$ and 8.8×10^{-4} mol/L KH_2PO_4 in deionised water.

2.3. Synthesis of SPAM material for CRT

2.3.1. Graphene oxide production—The first stage of the SPAM synthesis consisted in the preparation of graphene oxide (GO) by direct exfoliation of graphite powder (Figure 1). This was made by the modified Hummers method, in which 2.0g of natural graphite powder, 2.0g of KNO_3 and 6.0g of $KMnO_4$ were added slowly to 40mL of concentrated H_2SO_4, immersed in an ice bath at 0°C, under vigorous stirring. The obtained mixture was kept under stirring for 1h, below 35°C. After that, 160mL of deionised water was added drop wise to dilute the solution and the temperature increased to ~95°C and kept at this temperature for 15 min. The resulting mixture was poured into 240 mL of ultrapure water and then, 16mL of 30% H_2O_2 was added to this solution, giving rise to a yellow-brown suspension, with colloidal GO material and flocculating graphite oxidized particles.

2.3.2. Graphene oxide activation—The previous suspension (1mg/mL) was centrifuged at 5000 rpm for 5 min to remove the unexfoliated graphite oxide particles. After this, GO was activated by adding of 1.0 mL NHS aqueous solution 50mg/mL and 0.3 mL of fresh EDAC aqueous solution 10 mg/mL. This mixture was left stirring, continuously, at room temperature, for 30 min. After this, the activated GO particles flocculated and were separated by centrifugation, thoroughly washed with water and dried under a nitrogen atmosphere (brown powder).

2.3.3. CRT imprinting—The imprinted layer was produced by incubating 1.4 mg of activated GO particles in 0.050 mL CRT solution 8.0×10^{-4}mol/L prepared in 5.0×10^{-4}mol/L HEPES buffer, for 3h. The solid fraction was isolated by centrifugation, washed with buffer solution, and incubated next in 0.050 mL TRIS solution 1.0mol/L, also prepared in HEPES buffer, for about 30 min. The solid was again isolated by centrifugation, washed with buffer, and incubated next in charged functional monomers, 0.025 mL of VBTMA (1.6×10^{-3}mol/L) and 0.025 mL of SSA (1.6×10^{-3}mol/L), for 2.5h. Once again, the solid was separated, washed and incubated, at room temperature, for 2.5h, in 0.050 mL of a solution containing 8.0×10^{-3}mol/L EGDMA, 1.6×10^{-3}mol/L Vpi and 4.0×10^{-3}mol/L APS, prepared in buffer. The imprinted solid material was then washed with buffer and finally incubated in a solution of glacial acetic acid and SDS (1:1), at room temperature, for 12h. The solid was finally thoroughly washed with buffer solution and dried under a nitrogen atmosphere.

Non-imprinted material (NIMs) was also prepared as control, following an equivalent procedure, where the CRT solution prepared in HEPES buffer was replaced by only buffer.

2.4. FTIR and Raman analysis

The FTIR analysis was conducted by placing the solid material on the ATR diamond surface. The spectra were collected under room temperature/humidity control, after background correction. The number of scans for sample and background was set to 32. The x-axis ranged from 525 to 4000 cm^{-1} and y-axis shown as % transmittance. The resolution was 4000.

The Raman spectra were measured with an objective 50× Zeiss (NA=0.70) that in combination with this microscope lead to a laser spot at the sample of 500 nm. The laser power applied at the sample ranged between 0.5 mW and 3 mW. The confocal microscope operated in single spectrum mode, at wavelength of 532 nm, and the spectra were recorded as an extended scan.

2.5. Preparation of the electrodes

CRT selective membranes were obtained by preparing a cocktail solution of PVC with *o*NPOE (plasticizer, 1:3, w/w), together with 0.15 mg of ionophore (SPAM or NIM). Some membranes were also added of anionic or cationic additives (0.5 mg of TpClPB or *p*TOAB, respectively), according to the membrane composition indicated in table 1. The resulting mixture was mixed and dispersed in 2.0 mL of THF and casted over the conductive supports.

All selective membranes were applied drop wise over graphite conductive supports. The graphite support was prepared by filling the smaller end of a plastic syringe with a mixture of graphite and Araldite/hardener, and introducing a copper wire though this graphite-paste at the inner side of the syringe body. A small cavity was drilled externally on the hardened graphite to create a 1mm-deep cavity for applying the membrane.

Some of the selective membranes were casted similarly over ITO or FTO/ITO conductive flat supports. These supports were used as commercially available, cut into small pieces, washed with ethanol and dried. An electrical wire was linked to it by holding a copper wire against the conductive surface by means of insulating glue.

The applied membranes were let dry at room temperature, for 24h, and conditioned in a 1.0×10^{-3} mol/L CRT solution prior to emf readings.

2.6. Potentiometric assays

The electrodes were calibrated in HEPES buffer solution, 1.0×10^{-4}mol/L, by adding sample aliquots a standard 1.0×10^{-2}mol/L CRT solution, leading to CRT concentrations ranging from 1.0×10^{-6} to 1.7×10^{-3}mol/L. The emf was recorded after at stabilization to ±0.2mV and plotted as a function of logarithm CRT concentration.

Selectivity studies followed the Matched Potential Method, where CRT concentrations were set to 1.0×10^{-5}mol/L and increased up to 4.5×10^{-5}mol/L. The potential change depended of the electrode, with the most sensitive ones leading to a ~25mV decrease in emf. The interfering solutions tested were ascorbic acid (4.0g/L), BSA (15g/L), creatinine (30g/L), glucose (1.5g/L) and urea (2g/L), adding in small aliquots into a primary ion solution of CRT of 1.0×10^{-5}mol/L and producing concentrations changes up to their physiological level (BSA (3.9-5.0mg/L), creatinine (30g/L), glucose (10-100mg/L) and urea (<50 mg/L).

The analysis of CRT in urine samples was made in artificial urine solution spiked with CRT standard, diluted 1:10 diluted in HEPES buffer and analyzed by direct emf reading. The CRT concentrations so-obtained ranged from 2.0×10^{-6} to 2.8×10^{-3}mol/L.

3. Results and discussion

3.1. Design of SPAM material for CRT

The SPAM material was assembled on GO sheets obtained by graphite exfoliation (Figure 1). The analytical approach taken herein employed typical procedures described in the literature [36; 37], yielding a yellow-brown colloidal suspension. This suspension was composed of oxidized graphene sheets as colloidal material and was destabilized after the chemical activation of the carboxylic acid laying on the GO surface. This was done by well-known EDAC/NHS chemistry, yielding a labile *O*-acylisourea intermediate that was made evident by an immediate flocculation of the activated GO sheets. This flocculation further allowed a physical separation of the graphene-based material from the solution, by centrifugation and filtration.

The imprinting stage started by the physical interaction between CRT and activated GO material. Simple electrostatic interaction was allowed by complementary electrical environment between the positive charge of the quaternary ammonium salt in CRT and the negative polarity of oxygen atoms in the GO layer (Figure 1). Considering that CRT had a carboxylic function, anhydride bonding between CRT and the *O*-acylisourea intermediate become also possible (Figure 1). Since anhydride functions are quite unstable, this reaction allowed positioning the CRT over the receptor surface while allowing its easy removal after completing the imprinting stage. The inactivation of carboxylic acid functions that remained active was done by addition of TRIS, yielding amide bonds.

The GO/CRT material was incubated after in VBTMA (a positively charged monomer) and SSA (a negatively charged monomer). This incubation period had the purpose of

establishing ionic pairs between opposite charges: $-COO^{-}$//VBTMA and $-NR_3^{+}$//SSA (Figure 1). The vinyl group in the monomer structure would allow their participation in the subsequent polymerization stage and, consequently, position the charged group at the imprinted binding site. The polymerization was initiated by radical species (APS) and conducted with neutral vinyl-based materials. VPi and EGDMA were selected for this purpose (Figure 1). These compounds had only ester functions and acted as monomer and cross-linker, respectively.

Finally, CRT biomolecules in the polymeric matrix had to be removed in order to generate the binding sites and the so-called plastic antibody material. This was made by treatment the imprinted material with SDS and acetic acid. The final material was named SPAM and should display rebinding positions for CRT. In order to identify if this rebinding was being made by the specifically designed binding sites and/or non-specific interactions with the polymeric network, a control material was prepared with no CRT (named NIM), where only non-specific interactions were allowed.

3.2. Surface analysis of the host-tailored polymers

The chemical assembly of the imprinted layer on GO was followed by Raman spectroscopy and FTIR. The corresponding spectra were indicated in Figure 2A and 2B, respectively.

The Raman spectra of GO showed the typical G and D bands (Figure 2A), highlighting the hybridization of the carbon atoms as well as the electronic and geometrical carbon arrangement [38]. The G band is located at ~1580 cm^{-1} and corresponds to the stretching of the C–C bond in graphitic materials, common to all sp^2 carbon systems, while the D band appears at ~1370 cm^{-1}, assigning the presence of disorder in the sp^2-hybridized carbon system [38; 39; 40]. It is possible that the analyzed material also includes contaminant graphitic material from which GO was extracted. The introduction of an additional polymeric imprinted layer at GO, when the SPAM material was assembled, was expected to introduce additional disorder into the sp^2 carbon system. This may be identified by analyzing the I_D/I_G intensity ratio between the disorder-induced D-band and the Raman allowed G band [38]. The direct comparison between GO and SPAM Raman spectra confirmed the presence of additional disorder, with I_D/I_G intensity ratios changing from 0.93 to 1.04.

The FTIR spectra also confirmed significant chemical differences between GO and SPAM (Figure 2B). Regarding GO material, the oxidation of graphene leads to the occurrence of ether, hydroxyl, and carbonyl bonding on the aromatic carbon rings. The C=O stretching vibration is typically intense and was observed at 1689 cm^{-1}, a position accounting the presence of the aromatic rings from graphene. The typical C–O stretching vibration in carboxylic acid and ether functions range from 1300–1000cm^{-1} [41] for which the medium intensity peak at 1200 cm^{-1} may be assigned to this event. The O–H stretching was evidenced by the broad adsorption below 2500cm^{-1} and there was also evidence for a C=C stretching vibration in a small intensity peak at 1579 cm^{-1}. The addition of an imprinted material to GO introduced mostly saturated ester functions on the matrix, leading to significant changes in the FTIR spectra. In the SPAM material, the C=O stretching vibration was located at 1718 cm^{-1}, shifting the higher *x* values. The band due to the C–O–C

asymmetric stretching vibration occurred at 1219cm^{-1} and that due to the symmetric stretching vibration was evident at 1050cm^{-1}, as expected for aliphatic esters [41].

3.3. Effect of significant variables on the response of CRT selective electrodes

CRT selective electrodes were prepared with either SPAM (ISE I) or NIM (ISE II) materials acting as ionophore. These materials were dispersed in PVC dissolved in THF and plasticized by the addition of *o*NPOE, a high dielectric constant plasticizer solvent. Other membranes were prepared similarly, including a lipophilic ionic additive. Either positive (ISE III) or negatively (ISE V) charged additive was employed, considering that CRT has a constant positive charge at the nitrogen atom but may also bear a negative charge by acid/base ionization of the carboxylic acid function. Control membranes having these additives and no ionophore (ISE IV and VI) were also prepared to investigate the effect of the additive alone and identify the effect of the ionophore.

All these membranes were casted on electrode supports with graphite-based conductive material and the corresponding analytical features evaluated according to IUPAC recommendations (average results in table 2). The best membrane compositions were use to prepare similar devices employing alternative conductive supports.

3.3.1. Effect of membrane composition—The typical potentiometric response of the ISEs prepared on graphite-based conductive supports may be seen in Figure 3A. The results indicated that SPAM ionophore improved the overall analytical performance of the device compared to NIM, decreasing the concentration level to which the electrode became responsive. This was evident by direct comparison of ISEs I and II, displaying linear responses down to 76 or 96 μmol/L CRT, with average anionic slopes of −47 and −45 mV/decade and limits of detection (LODs) of 41 and 50 μmol/L, respectively.

The addition of a lipophilic anionic additive gave rise to a potentiometric response with a positive slope (ISE III), meaning that the response of the electrode was now dominated by positive charges. The SPAM material was the one acting as ionophore in this condition (and not the additive), because the additive alone (ISE IV) was unable to produce a consistent behavior (Figure 3A). The analytical response of ISE III also showed an unusual behavior by reaching early potential saturation, at ~1×10^{-4} mol/L. This response was considered a drawback at the future application of the device to the analysis of real samples. Contrasting to this behavior, the presence of the cationic lipophilic additive *p*TOBA improved the analytical performance of the electrodes, by decreasing the CRT concentration to which the electrode responded (ISE V). This effect was similar to that produced by the electrode having only additive (ISE VI), and therefore it was impossible to understand if this behavior resulted from the additive alone or the combination additive/SPAM ionophore.

Overall, the use of membranes composed by SPAM material favored the analytical response of the CRT selective electrodes and it was not clear if the presence of a lipophilic cationic additive would improve the performance of the devices.

3.3.2. Effect of pH—The pH of the analyzed solution may influence the potentiometric response. This is an outcome of the changes in the ionization degree of the carboxylate

group of CRT under different pH conditions and the kind of ionic species present in the electrolyte acting as buffer. Considering this combined effect, this study was conducted for buffers of different compositions, prepared at a specific concentration and without adding external species (thereby ensuring a higher buffer capacity under practical conditions). The buffers selected for this study were PIPES, MES, HEPES, PBS and MOPS, corresponding to 2.5, 4.1, 5.1, 7.4 and 9.2 pH values when set to a 5.0×10^{-3} mol/L concentration.

Electrodes including membranes with SPAM (I and III) or NIM (II or VII), and with additive (III and VI) or without additive it (I and II) were tested for the different pH/buffer conditions. As an example, the calibrations obtained with electrodes ISE I are presented in Figure 3B. Overall, more acidic pH conditions hindered the electrode performance, which was most probably correlated to the decreased ionization of the carboxylic acid function. Neutral or alkaline pH gave rise to steady potentials. This behavior could be attributed to the prevailing double ionization of CRT (zwitterionic form), resulting in the interaction of the membrane with a zero net charge species and consequently to no potential variation. The best pH condition was indeed the buffer used to test the membrane composition (HEPES, 5.1).

3.3.3. Effect of conductive support—The effect of the conductive support on the potentiometric response was tested by casting the selective membranes on conductive materials placed on plastic (PET) or glass supports. The conductive layers consisted of flat ITO or FTO/ITO surfaces, used as commercially available. Selective membranes including SPAM (I and III) or NIM (II or VII) ionophore, with additive (III and VI) or no additive (I and II) were selected for this purpose. The typical calibration curves obtained are depicted in Figure 4 and the corresponding features in table 2.

In general, significant changes were observed in the performance of the electrodes by changing the conductive support, with electrodes composed of SPAM material and anionic lipophilic additive (ISE V) showing significant improvements in sensitivity. These electrodes were the only ones showing an expanded linear concentration range and an increased sensitivity, both in conductive glass (Figure 4A) and plastic supports (Figure 4B). Interestingly (and strangely at the same time) membranes assembled on the conductive PET shifted the emf changes from negative to positive slopes. An upper limit of linear range was also identified, with limiting concentrations of 9.5×10^{-5}, 1.6×10^{-4} and 2.8×10^{-4} mol/L, for ISEs I, II and VII, respectively.

A disadvantageous feature associated to these new conductive supports was the decrease in stability of the emf readings and the worsened precision between consecutive calibrations (table 2). These features could be attributed to the simple fact that the membrane on this new flat conductive surface was thinner, which could accelerate emf drifts driven by the direct interaction of the hydration water molecules with the conductive material. The lifetime of the electrodes was smaller than those employing graphite-based supports.

3.4. Selectivity of the electrodes

Selectivity assays used the Matched Potential Method and tested the effect of species that may co-exist with CRT in urine (ascorbic acid, BSA, Crea, glucose and urea, among other

electrolytes), assessed up to their normal physiological concentration. For this purpose, several aliquots of standard solutions containing individual species were added to a solution of 1.0×10^{-5} or 4.6×10^{-4}mol/L in CRT, depending of the linear range of the electrode under study. The log values of the selectivity coefficients (K^{POT}) obtained are presented in Figure 5. The overall log K^{POT} values ranged −3.33/+0.25; −1.89/+0.52; and −1.71/+0.97 for conductive supports of graphite-based, FTO/ITO-glass and ITO-PET, respectively. When the interfering species was not able to introduce the necessary potential change, the log K^{POT} was calculated by using the maximum concentration of interfering species tested and co-existing with CRT in solution.

Regarding the graphite-based electrodes, the most selective readings have been recorded with ISEs containing negative lipophilic additive (ISEs III and IV). This occurrence did not mean, however, that these electrodes were the most selective; the range of concentration tested for these devices was different (lower, due to the linear range of response) and the emf values of these electrodes became stable at higher concentrations, thereby hindering the detection of an interfering effect. The electrodes with SPAM/NIM or cationic lipophilic additive showed similar behavior, suggesting that the additive did not affect the selectivity features of the devices. Moreover, the apparent interference from glucose (a non-ionic species) was linked to the use of glucose concentrations lower than those of CRT present, rather than an emf change caused by the addition of glucose. In fact, the total changes in emf values after glucose addition varied from a minimum of 3.0 mV (ISE II) to a maximum of 5.0 mV (ISE I).

The use of FTO/ITO-glass seemed to improve the selectivity of the ISEs compared to graphite-based devices (Figure 5B), with several species tested to their maximum concentration without causing the necessary potential change. The opposite effect was observed for ITO-PET based electrodes, leading to more positive log K^{POT} values (Figure 5C). The overall behavior pointed out better selectivity for ISEs I or V, especially when FTO/ITO-glass was used as conductive support.

3.4.1. Determination of CRT in urine—For the analytical application of the CRT selective electrodes, the ISEs V were selected because these were the ones combining the best selectivity and sensitivity. These electrodes also included a linear response within the average of normal carnitine concentration expected in urine. An average value of 18.8 and 9.3 mg/L in man and women, respectively, would be expected assuming reference values of carnitine in urine of 28.2mg/day (175micromol/day) in man or 13.9 mg/day (86micromol/day) in women, and urine average output per individual each day of about 1.5L.

The analysis was conducted after running a calibration of the ISEs in synthetic urine containing BSA and checking the analytical performance. The devices were applied to determine CRT in urine samples ranging from 3.4×10^{-4} to 1.3×10^{-4}mol/L. The response time of the electrodes was always below 30 seconds, independent of the concentration level used. The lifetime of the electrodes was three months. The obtained recoveries were of 91% (± 6.8%) to 118% (± 11.2%), respectively, with relative errors below −20% and a corresponding average relative standard deviation of 8.0%. A similar approach was taken for the same membrane casted on conductive glass, with similar results to those reported herein.

An estimate about false positives or negatives within sample analysis cannot be provided because there are individuals that may have abnormal urine component that have not been tested herein.

4. Conclusions

Novel SPAM materials were tailored on GO supports with charged monomers. These materials were successfully introduced in plasticized PVC membranes for potentiometric transduction made with electrodes of different conductive materials. Overall, the use selective membranes containing SPAM as ionophore and a cationic lipophilic additive favored the overall analytical performance of the final devices, providing suitable selectivity features for practical application, with fast response and improved LODs for this potential biomarker of ovarian cancer. This effect was enhanced by casting the membrane over a conductive glass support. Moreover, the obtained analytical data showed that the CRT sensors could be applied with success to the analysis of synthetic urine samples. Other advantages of these devices include simplicity, low cost, quick responses, high analytical throughput, low LOD and good selectivity.

Overall, the combination of SPAM sensory material designed for CRT with a suitable selective membrane composition and electrode design produced devices with suitable analytical performance for point-of-care application.

Acknowledgements

The authors acknowledge the financial support of European Research Council, through the Starting Grant 3P's given to MGFS (GA 311086). *Werfen Group - Izasa Portugal* and *WITec GmbH* is also acknowledged for the Raman Microscopy analysis of the SPAM materials.

References

[1]. Pormsila W, Morand R, Kraehenbuehl S, Hauser PC. Capillary electrophoresis with contactless conductivity detection for the determination of carnitine and acylcarnitines in clinical samples. Journal of Chromatography B-Analytical Technologies in the Biomedical and Life Sciences. 2011; 879:921–926.

[2]. Fong MY, McDunn J, Kakar SS. Identification of Metabolites in the Normal Ovary and Their Transformation in Primary and Metastatic Ovarian Cancer. Plos One. 2011; 6

[3]. Ahmed HH. Modulatory effects of vitamin E, acetyl-L-carnitine and alpha-lipoic acid on new potential biomarkers for Alzheimer's disease in rat model. Experimental and Toxicologic Pathology. 2012; 64:549–556. [PubMed: 21183322]

[4]. Calo LA, Pagnin E, Davis PA, Semplicini A, Nicolai R, Calvani M, Pessina AC. Antioxidant effect of L-carnitine and its short chain esters - Relevance for the protection from oxidative stress related cardiovascular damage. International Journal of Cardiology. 2006; 107:54–60. [PubMed: 16337498]

[5]. Flanagan JL, Simmons PA, Vehige J, Willcox MDP, Garrett Q. Role of carnitine in disease. Nutrition & Metabolism. 2010; 7

[6]. Chang BJ, Nishikawa M, Sato E, Utsumi K, Inoue M. L-Carnitine inhibits cisplatin-induced injury of the kidney and small intestine. Archives of Biochemistry and Biophysics. 2002; 405:55–64. [PubMed: 12176057]

[7]. Marzo A, Cardace G, Monti N, Muck S, Martelli EA. Chromatographic and nonchromatographic assay of l-carnitine family components. Journal of Chromatography-Biomedical Applications. 1990; 527:247–258. [PubMed: 2201692]

[8]. Marzo A, Monti N, Ripamonti M, Martelli EA. Application of high-performance liquid-chromatography to the analysis of propionyl-l-carnitine by a stereospecific enzyme assay. Journal of Chromatography. 1988; 459:313–317. [PubMed: 3243906]

[9]. Dabrowska M, Starek M. Analytical approaches to determination of carnitine in biological materials, foods and dietary supplements. Food Chemistry. 2014; 142:220–232. [PubMed: 24001835]

[10]. Kivilompolo M, Ohrnberg L, Oresic M, Hyotylainen T. Rapid quantitative analysis of carnitine and acylcarnitines by ultra-high performance-hydrophilic interaction liquid chromatography-tandem mass spectrometry. Journal of Chromatography A. 2013; 1292:189–194. [PubMed: 23336946]

[11]. Isaguirre AC, Olsina RA, Martinez LD, Lapierre AV, Cerutti S. Rapid and sensitive HILIC-MS/MS analysis of carnitine and acetylcarnitine in biological fluids. Analytical and Bioanalytical Chemistry. 2013; 405:7397–7404. [PubMed: 23877176]

[12]. Deng YZ, Henion J, Li JJ, Thibault P, Wang C, Harrison DJ. Chip-based capillary electrophoresis/mass spectrometry determination of carnitines in human urine. Analytical Chemistry. 2001; 73:639–646. [PubMed: 11217774]

[13]. Deng YZ, Zhang NW, Henion J. Chip-based quantitative capillary electrophoresis/mass spectrometry determination of drugs in human plasma. Analytical Chemistry. 2001; 73:1432–1439. [PubMed: 11321291]

[14]. Vernez L, Thormann W, Krahenbuhl S. Analysis of carnitine and acylcarnitines in urine by capillary electrophoresis. Journal of Chromatography A. 2000; 895:309–316. [PubMed: 11105876]

[15]. Hassett RP, Crockett EL. Endpoint fluorometric assays for determining activities of carnitine palmitoyltransferase and citrate synthase. Analytical Biochemistry. 2000; 287:176–179. [PubMed: 11078597]

[16]. Galan A, Padros A, Arambarri M, Martin S. Automation of a spectrophotometric method for measuring L-carnitine in human blood serum. Journal of Automatic Chemistry. 1998; 20:23–26. [PubMed: 18924818]

[17]. Yalkowsk, Sh; Zografi, G. Potentiometric titration of monomeric and micellar acylcarnitines. Journal of Pharmaceutical Sciences. 1970; 59:798. -&. [PubMed: 5423081]

[18]. Botre C, Botre F, Pranzoni C. A potentiometric approach to the study of the antagonism between acetazolamide and L-carnitine congeners on carbonic-anhydrase activity. Electroanalysis. 1991; 3:567–572.

[19]. Rat'Ko AA, Stefan RI, van Staden JF, Abould-Enein HY. Determination of l-carnitine using enantioselective, potentiometric membrane electrodes based on macrocyclic antibiotics. Talanta. 2004; 63:515–519. [PubMed: 18969462]

[20]. Stefan RL, Bokretsion RG, van Staden JF, Aboul-Enein HY. Determination of L- and D-enantiomers of carnitine using amperometric biosensors. Analytical Letters. 2003; 36:1091–1102.

[21]. Zeravik J, Teller C, Scheller FW. Analysis of cholinesterase binding to a carnitine-modified EQCM sensor. Biosensors & Bioelectronics. 2007; 22:2244–2249. [PubMed: 17174085]

[22]. Lesnik B. Immunoassay Techniques in Environmental Analyses. Encyclopedia of Analytical Chemistry. 2000:2653–2672.

[23]. Tan CJ, Chua MG, Ker KH, Tong YW. Preparation of bovine serum albumin surface-imprinted submicrometer particles with magnetic susceptibility through core-shell miniemulsion polymerization. Analytical Chemistry. 2008; 80:683–692. [PubMed: 18181645]

[24]. Tan CJ, Tong YW. Molecularly imprinted beads by surface imprinting. Analytical and Bioanalytical Chemistry. 2007; 389:369–376. [PubMed: 17563884]

[25]. Moreira FTC, Sharma S, Dutra RAF, Noronha JPC, Cass AEG, Sales MGF. Smart plastic antibody material (SPAM) tailored on disposable screen printed electrodes for protein recognition: Application to myoglobin detection. Biosensors & Bioelectronics. 2013; 45:237–244. [PubMed: 23500370]

[26]. Tavares APM, Moreira FTC, Sales MGF. Haemoglobin smart plastic antibody material tailored with charged binding sites on silica nanoparticles: its application as an ionophore in potentiometric transduction. Rsc Advances. 2013; 3:26210–26219.

[27]. Gauczinski J, Liu Z, Zhang X, Schoenhoff M. Surface Molecular Imprinting in Layer-by-Layer films on Silica Particles. Langmuir. 2012; 28:4267–4273. [PubMed: 22324368]

[28]. Cabral-Miranda G, Gidlund M, Sales MGF. Backside-surface imprinting as a new strategy to generate specific plastic antibody materials. Journal of Materials Chemistry B. 2014; 2:3087–3095.

[29]. Chen, PY.; Nien, PC.; Ho, KC. Highly Selective Dopamine Sensor based on an Imprinted SAM/Mediator Gold Electrode; Proceedings of the Eurosensors Xxiii Conference; 2009; p. 285-288.

[30]. Moreira FTC, Queiros RB, Truta LAA, Silva TI, Castro RM, Amorim LR, Sales MG. Host-Tailored Sensors for Leucomalachite Green Potentiometric Measurements. Journal of Chemistry. 2013

[31]. Zhang X-L, Zhang Y, Yin X-F, Du B-B, Zheng C, Yang H-H. A facile approach for preparation of molecularly imprinted polymers layer on the surface of carbon nanotubes. Talanta. 2013; 105:403–408. [PubMed: 23598037]

[32]. Kuila T, Bose S, Mishra AK, Khanra P, Kim NH, Lee JH. Chemical functionalization of graphene and its applications. Progress in Materials Science. 2012; 57:1061–1105.

[33]. Huang X, Yin Z, Wu S, Qi X, He Q, Zhang Q, Yan Q, Boey F, Zhang H. Graphene-Based Materials: Synthesis, Characterization, Properties, and Applications. Small. 2011; 7:1876–1902. [PubMed: 21630440]

[34]. Kamel AH, Coelho Moreira FT, Ribeiro Rebelo TS, Ferreira Sales MG. Molecularly-imprinted materials for potentiometric transduction: application to the antibiotic enrofloxacin. Analytical Letters. 2011; 44:2107–2123.

[35]. Singh AK, Gupta VK, Gupta B. Chromium(III) selective membrane sensors based on Schiff bases as chelating ionophores. Analytica Chimica Acta. 2007; 585:171–178. [PubMed: 17386662]

[36]. Hummers WS, Offeman RE. Preparation of grafhitic oxide. Journal of theAmerican Chemical Society. 1958; 80:1339.

[37]. Ge S, Yan M, Lu J, Zhang M, Yu F, Yu J, Song X, Yu S. Electrochemical biosensor based on graphene oxide-Au nanoclusters composites for L-cysteine analysis. Biosensors & Bioelectronics. 2012; 31:49–54. [PubMed: 22019101]

[38]. Dresselhaus MS, Jorio A, Hofmann M, Dresselhaus G, Saito R. Perspectives on Carbon Nanotubes and Graphene Raman Spectroscopy. Nano Letters. 2010; 10:751–758. [PubMed: 20085345]

[39]. Li Y, Li X, Dong C, Qi J, Han X. A graphene oxide-based molecularly imprinted polymer platform for detecting endocrine disrupting chemicals. Carbon. 2010; 48:3427–3433.

[40]. Tran Thanh T, Castro M, Kim TY, Suh KS, Feller J-F. Graphene quantum resistive sensing skin for the detection of alteration biomarkers. Journal of Materials Chemistry. 2012; 22:21754–21766.

[41]. Socrates, G. Infrared and Raman Characteristic Group Frequencies. John Wiley & Sons, Ltd; Chichester, UK: 2001.

Europe PMC Funders Author Manuscripts

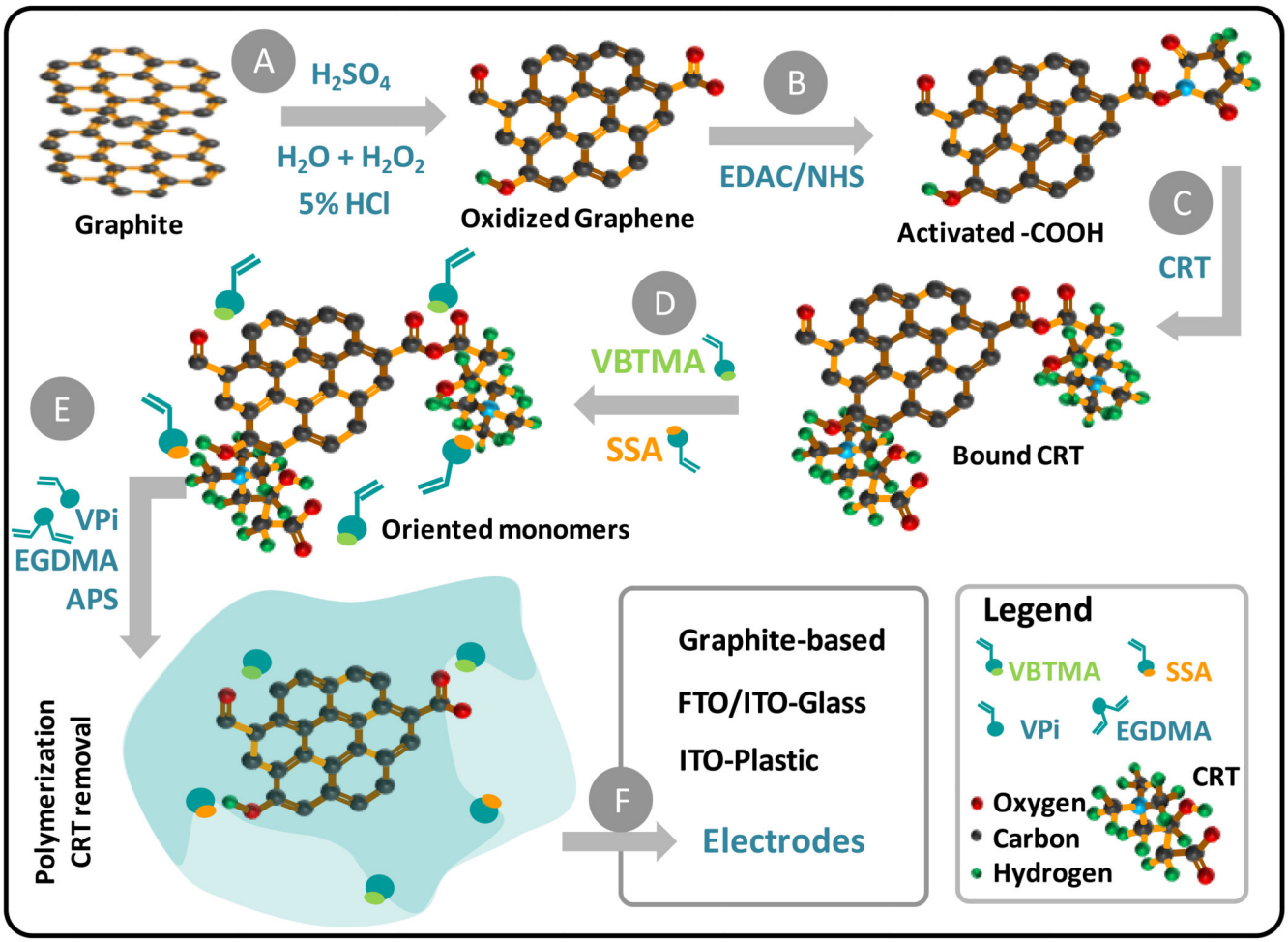

Figure 1.

Design of synthesis of CRT selective sensor. A: Preparation of GO by graphite exfoliation; B: Activation of carboxylic acid functions; C: Physiscal/Chemical interation with CRT; D: Charged monomer interaction with CRT; E: Polymerization around CRT with neutral material; F: application of the material in different conductive supports to prepared different CRT-selective electrodes.

Europe PMC Funders Author Manuscripts

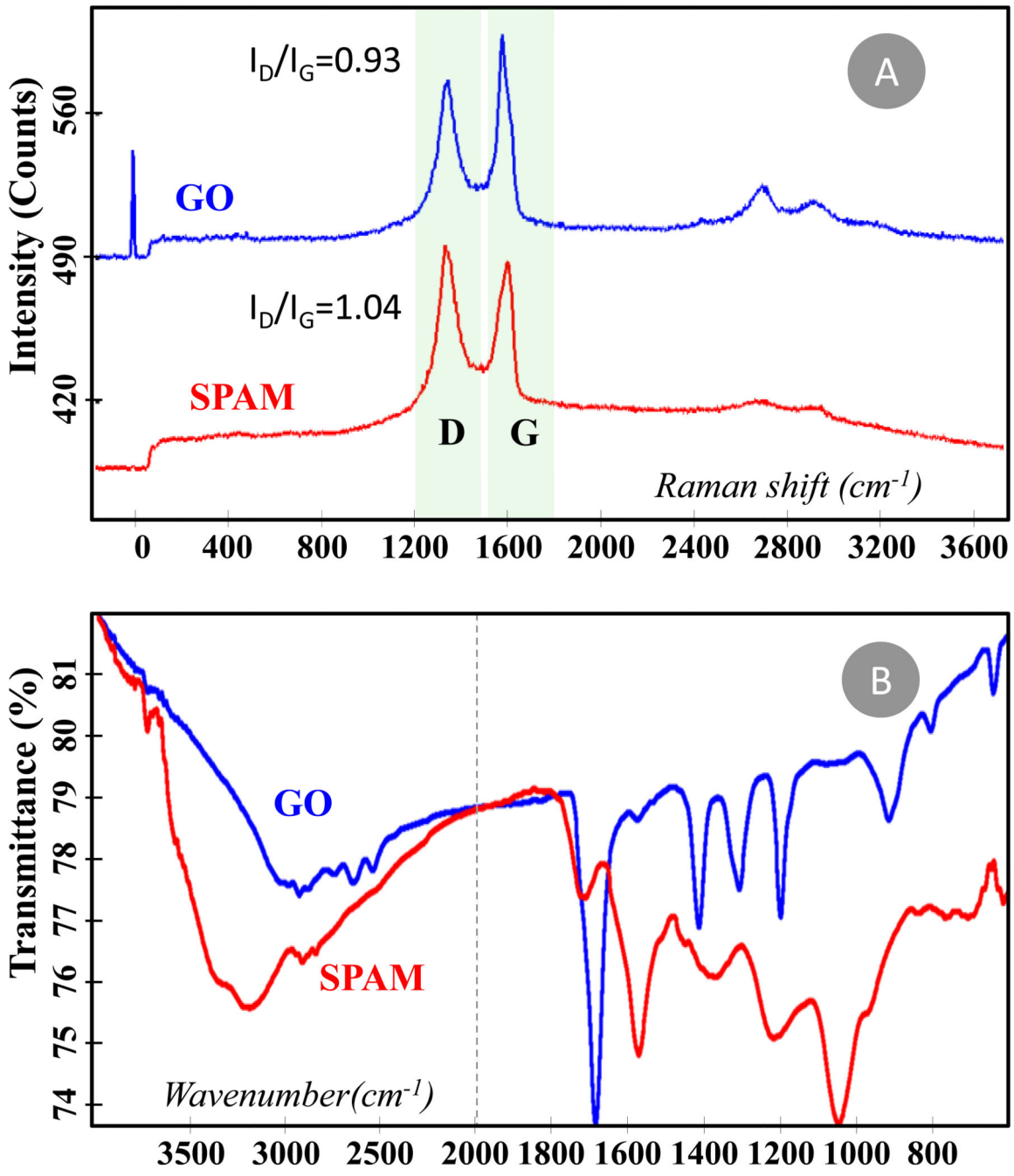

Figure 2.
Spectra of GO, SPAM and NIM materials. (A) Raman spectra, with bands G, D and 2D identified. (B) FTIR spectra.

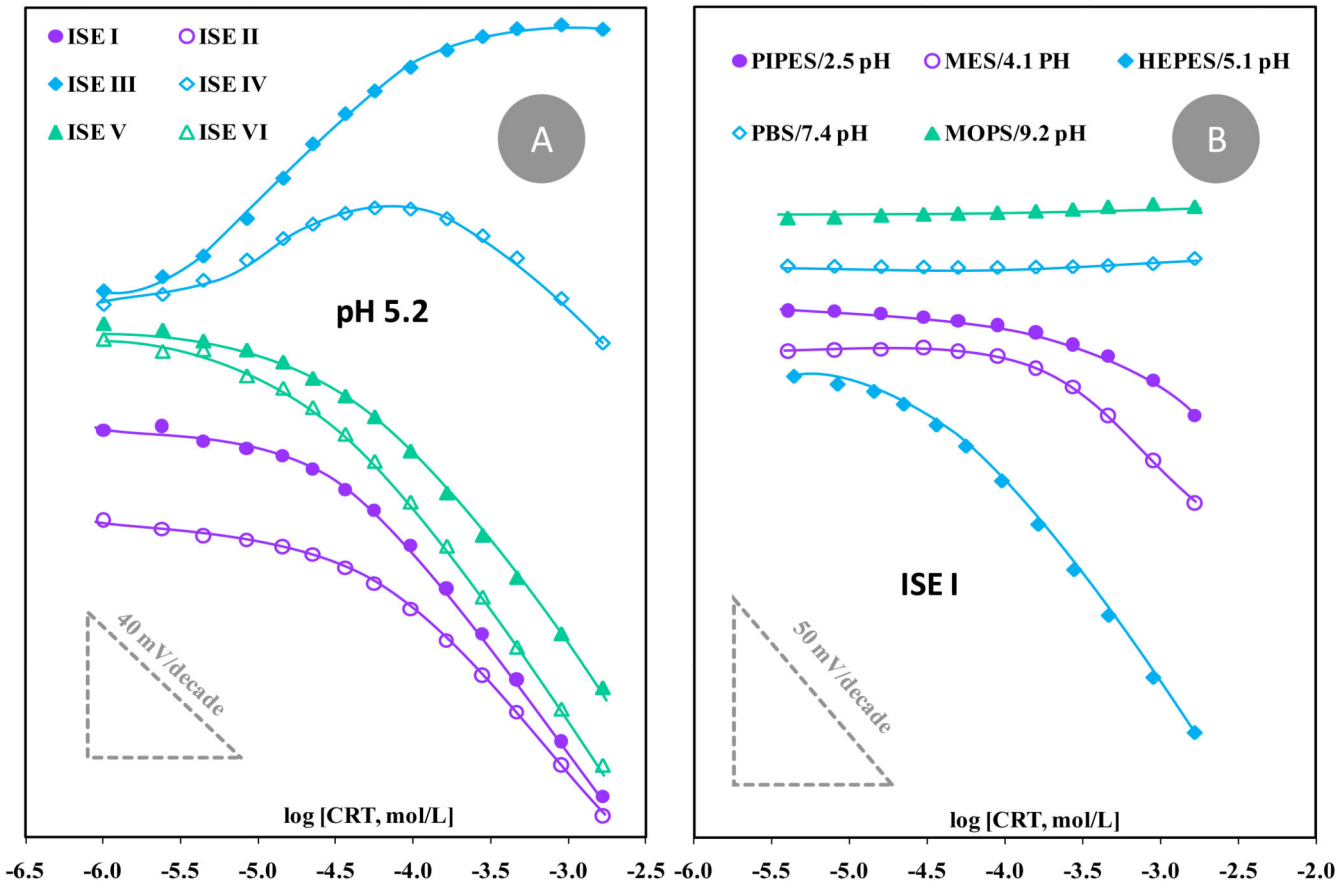

Figure 3.

Calibration of CRT selective electrodes with graphite-based conductive material. (A) Different membrane compositions evaluated in HEPES buffer pH 5.1. (B) Different buffer/pH conditions using ISE I.

Europe PMC Funders Author Manuscripts

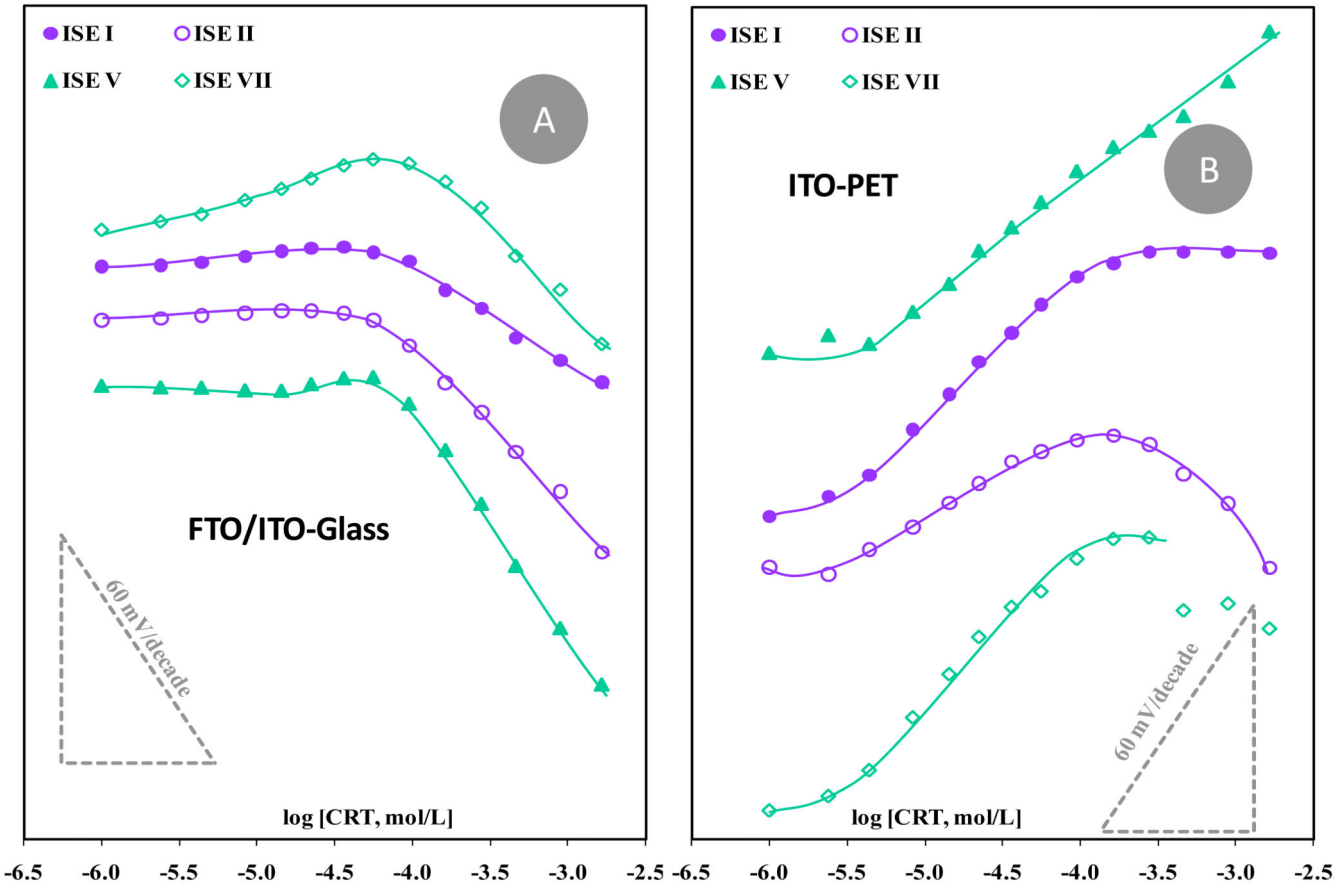

Figure 4.

Calibration of CRT selective electrodes with different selective membranes casted on conductive glass (A) or PET (B), and tested in HEPES buffer pH 5.1.

Europe PMC Funders Author Manuscripts

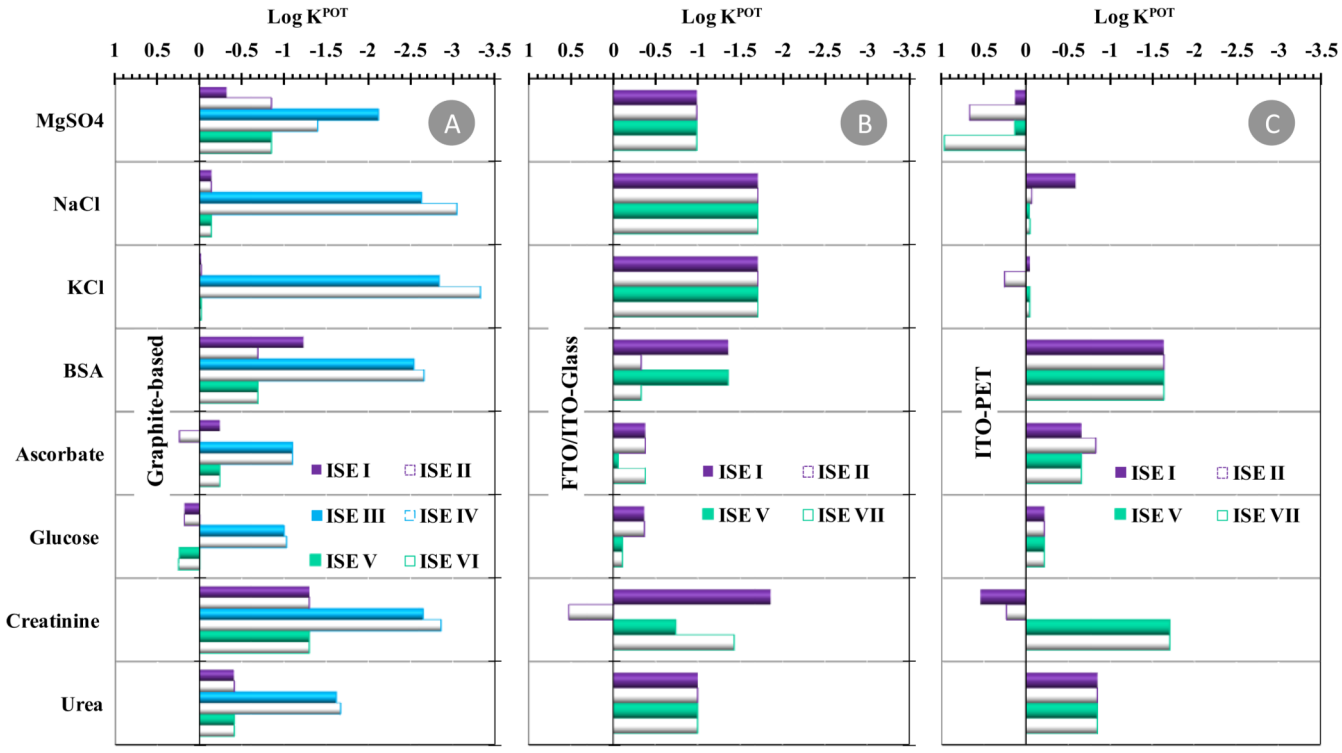

Figure 5.

Potentiometric selectivity coefficients of all electrodes,obtained by the matched potential method. (A) graphite-based; (B) FTO/ITO-glass; (C) ITO-PET.

Europe PMC Funders Author Manuscripts

Europe PMC Funders Author Manuscripts

Table 1

Membrane composition of all CRT selective-membranes, prepared by including ionophore and lipophilic additive in PVC membranes plasticized with *o*NPOE.

No.	*"Active" Components*		*Membrane composition (mg)*			
	Ionophore	*Additive*	*Ionophore*	*Plasticizer*	*Additive*	*PVC*
I	SPAM	—	0.13	5.60	—	2.21
II	NIM	—	0.15	18.19	—	2.27
III	SPAM	TpClPB	0.12	6.39	0.52	2.39
IV	—	TpClPB	—	9.46	0.53	2.36
V	SPAM	*p*TOAB	0.15	7.13	0.49	2.34
VI	—	*p*TOAB	—	9.28	0.50	2.36
VII	NIM	*p*TOAB	0.15	2.20	0.08	3.50

Europe PMC Funders Author Manuscripts

Table 2

Membrane composition of CRT sensors and the potentiometric features in 1.0×10^{-4}mol/L HEPES buffer, pH 5.2, with graphite-based electrodes.

Conductive support	Membrane system				Analytical features							
	No.	Ionophore	Plasticizer	Additive	Slope (mV/decade)	r^2 (n=3)	σ		LOD		LLLR	
							mV	mol/L	mol/L	mg/L	mol/L	mg/L
Graphite	*I*	SPAM	*o*NPOE	—	−47.2±5.9	0.9975	± 1.0	8.9×10^{-4}	4.1×10^{-5}	6.61	7.6×10^{-5}	12.25
	II	NIM	*o*NPOE	—	−44.6±4.7	0.9954	± 0.6	8.9×10^{-4}	5.0×10^{-5}	8.06	9.6×10^{-5}	15.48
	III	SPAM	*o*NPOE	TpClPB	+47.3±11.1	0.9968	± 0.6	1.6×10^{-4}	3.6×10^{-6}	0.58	4.4×10^{-6}	0.71
	IV	—	*o*NPOE	TpClPB	—	—	—	—	—	—	—	—
	V	SPAM	*o*NPOE	*p*TOAB	−45.1±2.7	0.9923	± 0.1	2.7×10^{-4}	3.9×10^{-5}	6.29	5.6×10^{-5}	9.03
	VI	—	*o*NPOE	*p*TOAB	−46.2±6.3	0.9950	± 0.3	4.6×10^{-4}	3.6×10^{-5}	5.80	5.6×10^{-5}	9.03
FTO/ITO-Glass	*I*	SPAM	*o*NPOE	—	−22.6±19.2	0.9958	± 2.2	1.7×10^{-3}	8.9×10^{-5}	14.35	9.5×10^{-5}	15.31
	II	NIM	*o*NPOE	—	−42.4±8.7	0.9958	± 0.1	2.8×10^{-4}	5.0×10^{-5}	8.06	5.6×10^{-5}	9.03
	V	SPAM	*o*NPOE	*p*TOAB	−57.4±3.7	0.9994	± 0.6	9.0×10^{-4}	6.3×10^{-5}	10.16	9.5×10^{-5}	15.31
	VII	NIM	*o*NPOE	*p*TOAB	−32.1±10.8	0.9917	± 2.6	9.5×10^{-5}	6.8×10^{-5}	10.96	1.7×10^{-4}	27.40
ITO/PET	*I*	SPAM	*o*NPOE	—	+37.61±1.78	0.9944	± 0.2	5.6×10^{-5}	2.3×10^{-6}	0.37	4.4×10^{-6}	0.71
	II	NIM	*o*NPOE	—	+20.24±2.44	0.9981	± 0.6	4.4×10^{-6}	1.3×10^{-6}	0.21	2.4×10^{-6}	0.39
	V	SPAM	*o*NPOE	*p*TOAB	+41.50±10.2	0.9964	± 4.7	1.4×10^{-5}	1.8×10^{-6}	0.29	2.4×10^{-6}	0.39
	VII	NIM	*o*NPOE	*p*TOAB	+34.53±18.4	0.9921	± 2.0	4.4×10^{-6}	2.8×10^{-5}	4.51	4.4×10^{-6}	0.71

LOD: Limit of Detection; LLLR: Lower Limit of Linear Range; r^2: Squared correlation coefficient; RSD: Relative Standard Deviation.